

ULTRACAM photometry of the eclipsing cataclysmic variable OU Vir

W. J. Feline,¹* V. S. Dhillon,¹ T. R. Marsh,^{2,3} M. J. Stevenson,¹ C. A. Watson¹ and C. S. Brinkworth³

¹Department of Physics and Astronomy, University of Sheffield, Sheffield, S3 7RH, UK

²Department of Physics, University of Warwick, Coventry CV4 7AL, UK

³Department of Physics and Astronomy, University of Southampton, Southampton, SO17 1BJ, UK

Accepted for publication in the Monthly Notices of the Royal Astronomical Society

ABSTRACT

We present high-speed, three-colour photometry of the faint eclipsing cataclysmic variable OU Vir. For the first time in OU Vir, separate eclipses of the white dwarf and bright spot have been observed. We use timings of these eclipses to derive a purely photometric model of the system, obtaining a mass ratio of $q = 0.175 \pm 0.025$, an inclination of $i = 79.2 \pm 0.7$ and a disc radius of $R_d/a = 0.2315 \pm 0.0150$. We separate the white dwarf eclipse from the lightcurve and, by fitting a blackbody spectrum to its flux in each passband, obtain a white dwarf temperature of $T = 13900 \pm 600$ K and a distance of $D = 51 \pm 17$ pc. Assuming that the primary obeys the Nauenberg (1972) mass-radius relation for white dwarfs and allowing for temperature effects, we also find a primary mass $M_w/M_\odot = 0.89 \pm 0.20$, primary radius $R_w/R_\odot = 0.0097 \pm 0.0031$ and orbital separation $a/R_\odot = 0.74 \pm 0.05$.

Key words: binaries: close – binaries: eclipsing – stars: dwarf novae – stars: individual: OU Vir – novae: cataclysmic variables

1 INTRODUCTION

Cataclysmic variable stars (CVs) are short-period binary systems which typically consist of a cool main-sequence star transferring mass via a gas stream and accretion disc to a white dwarf primary. The impact of the stream with the accretion disc forms a so-called ‘bright spot’, which in systems that are significantly inclined to our line of sight can cause a rise in the observed flux as this region rotates into view, resulting in an ‘orbital hump’ in the lightcurve. In high-inclination systems eclipses of the white dwarf, bright spot and disc by the red dwarf secondary can also occur. Analysis of these eclipses can yield determinations of system parameters such as the mass ratio q , the orbital inclination i and the radius of the accretion disc R_d (e.g. Wood et al. 1989). Eclipsing systems are therefore valuable sources of data on CVs.

Dwarf novae are a sub-type of CVs which show intermittent luminosity increases of 2–5 magnitudes, known as outbursts. A further sub-type of dwarf novae are the SU UMa stars, which exhibit superoutbursts at regular intervals, during which the luminosity increases by ~ 0.7 mag-

nitudes over the normal outburst maximum. These superoutbursts are characterised by the presence of superhumps – increases in brightness that usually recur at a slightly longer period than the orbital cycle. There is found to be a relationship between this superhump period excess ϵ and the mass ratio (Patterson 1998). Determinations of the mass ratios of SU UMa stars are therefore useful to calibrate this relation, which can then be used to determine the mass ratios of other SU UMa stars.

OU Vir is a faint ($V \sim 18$; Mason et al. 2002) eclipsing CV with a period of 1.75 hr which has been seen in outburst and probably superoutburst (Vanmunster et al. 2000), marking it as a SU UMa dwarf nova. Mason et al. (2002) presented time-resolved, multi-colour photometry and spectroscopy of OU Vir, concluding that the eclipse is of the bright spot and disc, but not the white dwarf. In this paper we present lightcurves of OU Vir, obtained with ULTRACAM, an ultra-fast, triple-beam CCD camera; for more details see Dhillon & Marsh (2001); Dhillon et al. (2003).

* E-mail: w.feline@shef.ac.uk

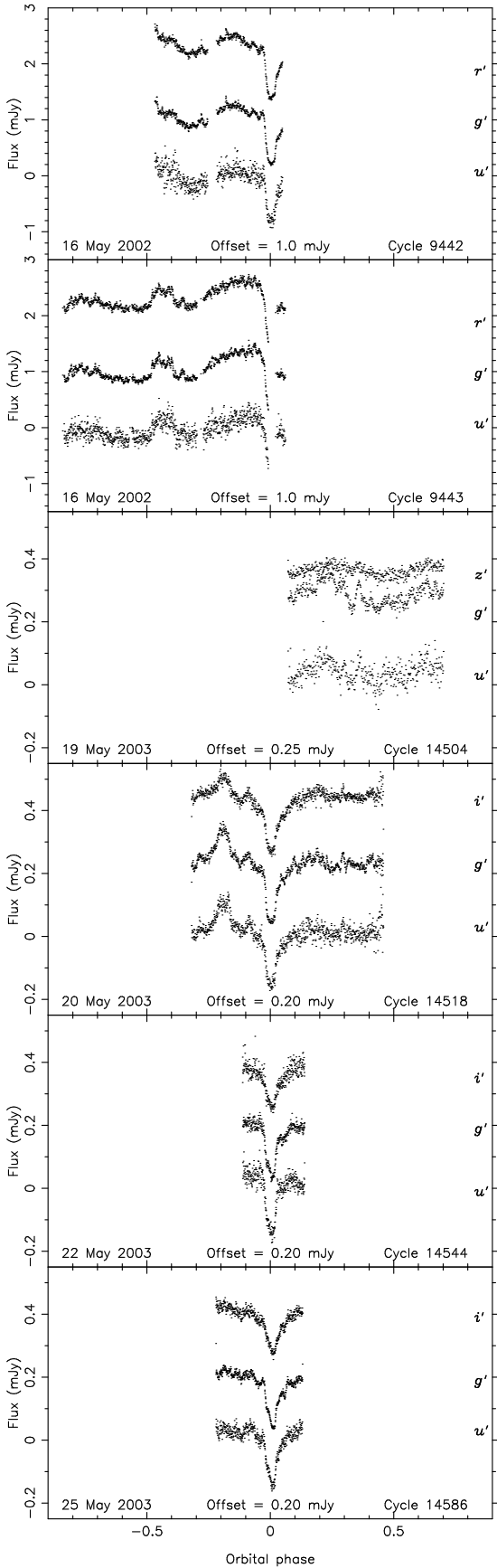


Figure 1. The lightcurve of OU Vir. The r' , z' or i' data are offset vertically upwards and the u' data are offset vertically downwards.

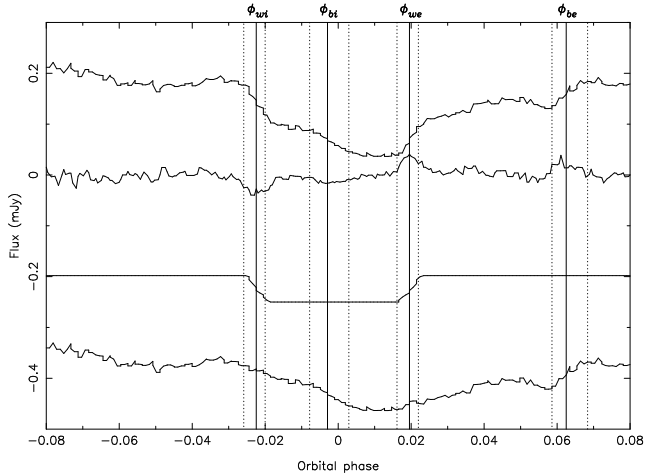


Figure 2. White dwarf deconvolution of the g' band lightcurve of 25 May 2003. Top to bottom: The data after smoothing by a median filter; the derivative after smoothing by a box car filter and subtraction of the spline fit to this, multiplied by a factor of 5 for clarity; the reconstructed white dwarf lightcurve, shifted downwards by 0.25 mJy; the original lightcurve minus the white dwarf lightcurve after smoothing by a median filter, shifted downwards by 0.5 mJy. The vertical lines show the contact phases of the white dwarf and bright spot eclipses, the dotted lines corresponding to $\phi_{w1} \dots \phi_{w4}$, $\phi_{b1} \dots \phi_{b4}$ and the solid lines (labelled) to ϕ_{wi} , ϕ_{we} and ϕ_{bi} , ϕ_{be} . The bright spot ingress and egress are plainly visible, quickly following the white dwarf ingress and egress respectively.

2 OBSERVATIONS

OU Vir was observed on the nights of 16 May 2002 and 19, 20, 22 and 25 May 2003 using ULTRACAM on the 4.2-m William Herschel Telescope (WHT) at the Isaac Newton Group of Telescopes, La Palma. The observations were obtained simultaneously in the r' , g' , and u' colour bands on the 16 May 2002, the z' , g' , and u' bands on the 19 May 2003, and the i' , g' , and u' bands on subsequent nights. Data reduction was carried out using the ULTRACAM pipeline data reduction software. Unfortunately, we were unable to observe a standard star in the z' band using ULTRACAM, so the zeropoint for this filter was chosen to be the same as for the i' band; this will only affect the scale of the z' lightcurve, not its shape. All the data were corrected to zero airmass using the nightly extinction coefficients measured by the Carlsberg Meridian Telescope on La Palma in the r' filter, and converted to other colour bands using the procedure described by King (1985) and the effective wavelengths of the filters given by Fukugita et al. (1996).

The lightcurves of OU Vir are shown in Figure 1. On 16 May 2002 the exposure time was 0.5 seconds and the data points were separated by approximately 4.9 seconds. These data were obtained on the first night of commissioning and hence were adversely affected by typical commissioning problems, chiefly excess noise in the u' band and limited time resolution due to the dead-time between exposures. The data taken in 2003 had no such problems, and hence the dead-time was reduced to 0.025 seconds. The exposure times for these observations varied according to the seeing on the night, and were 9.2 seconds on 19 May 2003, 5.2 seconds on 20 May 2003 and 4.2 seconds thereafter.

3 LIGHTCURVE MORPHOLOGY

OU Vir was observed during descent from superoutburst in both 2002 and 2003. Mason et al. (2002) found that for OU Vir out of eclipse and during quiescence, $V = 18.08$ and $B - V = 0.14$, which corresponds to $g' \sim 0.2$ mJy (Smith et al. 2002). Vanmunster et al. (2000) quote an outburst amplitude of approximately 4 magnitudes (corresponding to a peak g' flux of ~ 8.4 mJy). The system appears to be significantly below superoutburst maximum on the 16 May 2002, and almost at its quiescent brightness during the 2003 observations: The maximum superoutburst flux we have observed is ~ 1.2 mJy on 16 May 2002, and the out-of-eclipse quiescent flux is ~ 0.2 mJy on 22 and 25 May 2003.

As the descent from superoutburst is typically much slower than the ascent, we suspect the 2002 observations took place during the former state, but of course we cannot be certain. The 2002 data are, as far as we are aware, the only observations of this superoutburst. The 2003 superoutburst was first reported on 2 May (Kato 2003). The superhump is visible in both the 16 May 2002 lightcurve at phase ~ -0.45 and the 20 May 2003 lightcurve at phase ~ -0.2 , but is not visible in later data, either because it had faded or it was at a phase which was not observed.

The lower three panels of Figure 1 show changes in the eclipse morphology that occur during the descent from superoutburst. Importantly, the eclipse morphology changed drastically from a single sharp ingress and egress on 20 May 2003, to separate eclipses of the white dwarf and bright spot in the u' and g' bands on 25 May 2003. The bright spot ingress is also visible in the g' data of 22 May 2003. (The second egress feature visible in this lightcurve is more gradual than it appears in the compressed scale of Figure 1, and is mainly due to the egress of the disc.) This evolution of the eclipse morphology is typical for a system going from (super) outburst to quiescence (see, for example, Rutten et al. 1992).

4 ECLIPSE CONTACT PHASES

The white dwarf eclipse contact phases given in Tables 1 and 2 were determined using the techniques described by Wood, Irwin & Pringle (1985), Wood et al. (1986) and Wood et al. (1989). A median filter was used to smooth the data, the derivative of which was then calculated numerically. A box-car filter was applied to this derivative, and simple searches were made to locate the minimum and maximum values of the derivative corresponding to the midpoints of ingress ϕ_i and egress ϕ_e . (In fact this method locates the steepest part of the ingress and egress, but we would expect these to correspond to the midpoints unless the light distribution is asymmetrical.) If a bright spot eclipse is also present, care must be taken to ensure that at this stage the ingress and egress of the white dwarf are not confused with those of the bright spot. The eclipse contact phases corresponding to the start and end of the ingress ϕ_1, ϕ_2 and the start and end of the egress ϕ_3, ϕ_4 were determined by locating the points where the derivative differs significantly from a spline fit to the more slowly varying component.

Once the white dwarf eclipse contact phases have been

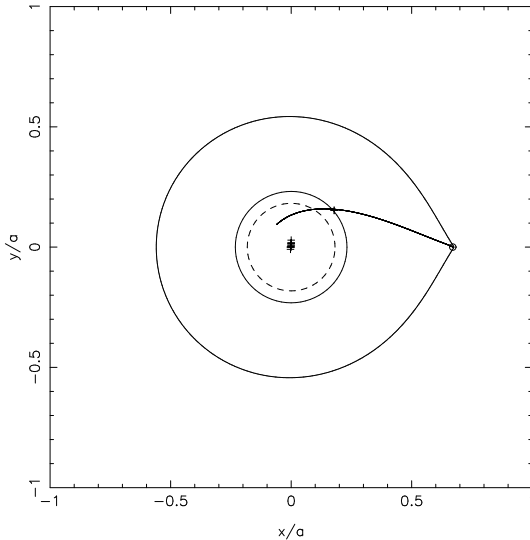


Figure 3. Trajectory of the gas stream from the secondary star for $q = 0.175$ and $i = 79^\circ 2$. Top: The system with the primary Roche lobe, L_1 point and disc of radius $R_d = 0.2315a$ plotted. The positions of the white dwarf and bright spot light centres corresponding to the observed ingress and egress phases for q and i as above are also plotted. The circularisation radius (Verbunt 1988, equation 13) of $R_{circ} = 0.1820a$ is shown as a dashed circle. The stream passes through the bright spot points (note that the timings of 22 May 2003 are of the ingress only which prevents it from being plotted).

found, the white dwarf lightcurve can be reconstructed and subtracted from the overall lightcurve as illustrated in Figure 2. The out-of-eclipse white dwarf fluxes thus found are given in Table 2. The white dwarf flux can be used to determine its temperature and distance; see section 6. Once this has been done the bright spot eclipse contact phases (given in Table 3) can be determined by a similar method (Wood et al. 1989) and its lightcurve removed from that of the disc eclipse. If successful, this process can be used to determine the bright spot temperature. Unfortunately we were unsuccessful in our attempts to do this, probably because flickering hindered accurate determination of the bright spot flux and contact phases.

In the discussion that follows we use the suffixes '*w*' and '*b*' to denote white dwarf and bright spot contact phases, respectively (e.g. ϕ_{wi} means the mid-ingress point of the white dwarf eclipse).

5 ORBITAL EPHEMERIS

A linear least-squares fit to the times of mid-eclipse given in Table 1 (calculated using the techniques described in section 4 and taking the midpoint of the white dwarf eclipse as the point of mid-eclipse) and those of Vanmunster et al. (2000, private communication) gives the following ephemeris:

$$HJD = 2451725.03283 + 0.072706113 \cdot E. \\ 7 \pm 5$$

Errors of $\pm 4 \times 10^{-5}$ days were used for the ULTRACAM data, and errors of $\pm 7 \times 10^{-4}$ days for the Vanmunster et al.

Table 1. Mid-eclipse timings.

Date	HJD			
	u'	g'	r'	i'
16 May 2002	2452411.523977	2452411.523921	2452411.523892	—
20 May 2003	2452780.580157	2452780.580278	—	2452780.580217
22 May 2003	2452782.470534	2452782.470558	—	2452782.470509
25 May 2003	2452785.524083	2452785.524083	—	2452785.524255

Table 2. White dwarf contact phases and flux.

Date	Band	ϕ_{w1}	ϕ_{w2}	ϕ_{w3}	ϕ_{w4}	ϕ_{wi}	ϕ_{we}	Flux (mJy)
16 May 2002	u'	-0.024414	-0.017578	0.018555	0.025391	-0.020508	0.022461	—
	g'	-0.027344	-0.018555	0.016602	0.025391	-0.022461	0.021484	—
	r'	-0.028320	-0.013672	0.012695	0.027344	-0.020508	0.020508	—
20 May 2003	u'	-0.023438	-0.016602	0.018555	0.025491	-0.019531	0.022461	—
	g'	-0.025391	-0.017578	0.017578	0.024414	-0.021484	0.021484	—
	i'	-0.023438	-0.014648	0.016602	0.025391	-0.018555	0.021484	—
22 May 2003	u'	-0.024414	-0.016602	0.017578	0.025391	-0.020508	0.021484	—
	g'	-0.026367	-0.018555	0.016602	0.024414	-0.022461	0.020508	—
	i'	-0.021484	-0.018555	0.016602	0.020508	-0.019531	0.018555	—
25 May 2003	u'	-0.025391	-0.016602	0.014648	0.023438	-0.020508	0.019531	0.0537
	g'	-0.025391	-0.019531	0.016602	0.022461	-0.022461	0.019531	0.0519
	i'	-0.022461	-0.018555	0.017578	0.022461	-0.020508	0.020508	0.0146

(2000, private communication) data. This ephemeris was used to phase all of our data.

6 SYSTEM PARAMETERS

The derivation of the system parameters relies upon the fact that there is a unique relationship between the mass ratio and orbital inclination for a given eclipse phase width $\Delta\phi = \phi_{we} - \phi_{wi}$:

- (i) At smaller orbital inclinations a larger secondary radius R_r is required in order to produce a given eclipse width.
- (ii) The secondary radius is defined by the mass ratio because the secondary fills its Roche lobe.
- (iii) Therefore for a specific white dwarf eclipse width, the inclination is known as a function of the mass ratio.

The shape of the system does not depend on the orbital separation a ; this just determines the scale. The orbital separation is determined by assuming a mass-radius relation for the primary (see later).

The trajectory of the gas stream originating from the inner Lagrangian point L_1 is calculated by solving the equations of motion (Flannery 1975) using a second-order Runge–Kutta technique and conserving the Jacobi Energy to 1 part in 10^4 . This assumes that the gas stream follows a ballistic path. Figure 3 shows a theoretical gas stream for $q = 0.175$. Figures 4 and 5 show expanded views of the bright spot region. As q decreases, the path of the stream moves away from the white dwarf. For a given mass ratio q each point on the stream has a unique phase of ingress and egress.

For each phase, the limb of the secondary forms an arc when projected along the line of sight onto a given plane

(hereafter referred to as a phase arc): each point on an individual phase arc is eclipsed at the same time. The intersection of the phase arcs corresponding to the respective eclipse contact phases can be used to constrain the size of the white dwarf and the structure of the bright spot. The light centres of the white dwarf and bright spot must lie at the intersection of the phase arcs corresponding to the relevant phases of mid-ingress and mid-egress, ϕ_i and ϕ_e . The phase arcs were calculated using full Roche lobe geometry rather than an approximate calculation.

The mass ratio and hence the inclination may be determined by comparing the bright spot light centres corresponding to the measured eclipse contact phases ϕ_{wi} and ϕ_{we} with the theoretical stream trajectories for different mass ratios q . This requires the assumption that the gas stream passes directly through the light centre of the bright spot. As illustrated in Figures 4 and 5, we constrain the light centre of the bright spot to be the point where the gas stream and outer edge of the disc intersect, so that the distance from the primary at which the gas stream passes through the light centre of the bright spot gives the relative outer disc radius R_d/a .

The bright spot timings thus yield a mass ratio of $q = 0.175 \pm 0.025$ and an inclination of $i = 79.2 \pm 0.7$ for an eclipse phase width $\Delta\phi = 0.041585$. The errors are determined by the rms variations in the measured contact phases. Figures 4 and 5 show the eclipse constraints on the structure of the bright spot. We use these to determine upper limits on the angular size and the radial and vertical extent of the bright spot, defining

$$\Delta\theta = (\theta_{23} + \theta_{24} - \theta_{13} - \theta_{14})/2 \quad (1)$$

$$\Delta R_d = (R_{24} + R_{14} - R_{23} - R_{13})/2 \quad (2)$$

$$\Delta Z = (H_{23} - H_{14})/2, \quad (3)$$

Table 3. Bright spot contact phases.

Date	Band	ϕ_{b1}	ϕ_{b2}	ϕ_{b3}	ϕ_{b4}	ϕ_{bi}	ϕ_{be}
22 May 2003	g'	-0.002930	0.002930	—	—	0.000977	—
25 May 2003	u'	-0.007813	0.002930	0.060547	0.065430	-0.002930	0.062500
	g'	-0.007813	0.002930	0.058594	0.068359	-0.002930	0.062500

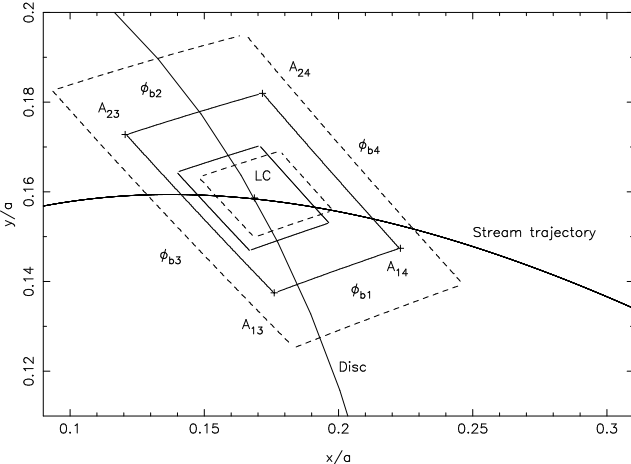


Figure 4. Horizontal structure of the bright spot for $q = 0.175$, showing the region on the orbital plane within which the bright spot lies. The light centre LC is marked by a cross, surrounded by the inner solid box which corresponds to the rms variations in position. The phase arcs which correspond to the bright spot contact phases are shown as the outer solid box, with the rms variations in position shown as the two dashed boxes. As all the timings of ϕ_{b2} and ϕ_{be} are identical, the rms variations of ϕ_{b1} and ϕ_{bi} respectively have been used instead. Intersections of the phase arcs ϕ_{bj} and ϕ_{bk} are marked A_{jk} , with crosses. The stream trajectory and disc of radius $R_d = 0.2315a$ are also plotted as solid curves.

where R_{jk} and θ_{jk} are the radius and azimuth of A_{jk} and H_{jk} the height of Z_{jk} above the orbital plane, as defined in Figures 4 and 5. θ increases in the direction of orbital motion and is zero at the line joining the centres of the two stars. Note that the definition of ΔZ in equation 3 differs slightly to that defined in Wood et al. (1986): this is in order to be more consistent with the definitions of $\Delta\theta$ and ΔR_d in equations 1 and 2. The mean position and extent of the bright spot are given in Table 4.

From Figures 4 and 5 we estimate that the gas stream passing through the light centre of the bright spot could just touch the phase arcs corresponding to ϕ_{b1} and ϕ_{b4} for a stream of circular cross-section with a radius $\varepsilon/a = 0.0175 \pm 0.0025$. The bright spot appears to be more extended azimuthally than radially, which can be understood by the shock front extending both up-disc and down-disc from the point of impact. The size of the stream is similar to that expected from theoretical studies (Lubow & Shu 1975, 1976) and that obtained by studies of similar objects (Wood et al. 1986, 1989), so our assumption that the stream passes through the light centre of the bright spot is reasonable.

Figure 6 shows the eclipse constraints on the radius of the white dwarf. Using the mass ratio and orbital inclination

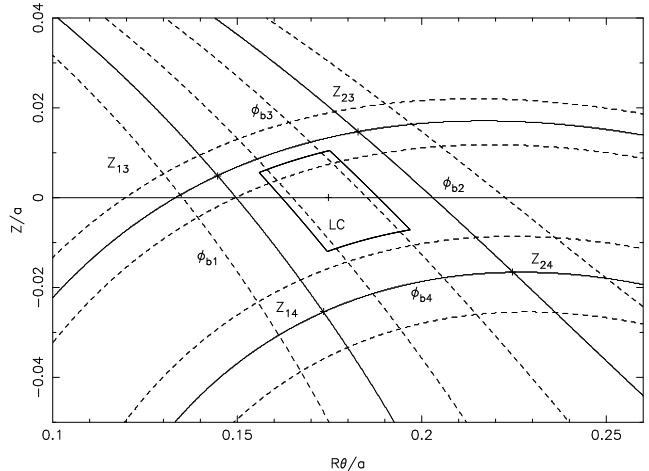


Figure 5. As Figure 4, but showing the vertical structure of the bright spot. The phase arcs are projected onto a vertical cylinder of radius $0.2315a$ (equal to that of the disc), i.e. the x -axis is stepping around the edge of the disc. θ is in radians. The intersections of the phase arcs ϕ_{bj} and ϕ_{bk} are marked Z_{jk} , with crosses.

derived earlier, we find that the white dwarf has a radius of $R_w = 0.013 \pm 0.004a$. An alternative possibility is that the sharp eclipse is caused by a bright inner disc region or boundary layer of radius $R_{belt} = 0.023 \pm 0.010a$ surrounding the white dwarf like a belt. These errors are calculated using the rms variations in the measured contact phases. Another possibility is that the lower hemisphere of the white dwarf is obscured by an optically thick accretion disc, which would result in the white dwarf radius being $R_w \geq 0.013a$. This is not the case, however, as the contact phases ϕ_{wi} and ϕ_{we} lie half-way through the white dwarf ingress and egress (see section 4), i.e. the light centre in Figure 6 lies at the origin and the light distribution is symmetrical.

The following analysis assumes that the eclipse is of a bare white dwarf. If the eclipse is actually of a belt and the white dwarf itself is not visible, then the white dwarf radius must be smaller than $R_{belt} = 0.023a$. If the white dwarf does contribute significantly to the eclipsed light, then we have the additional constraint that its radius must be $R_w \leq 0.013a$, so that the white dwarf mass given in Table 5 is actually a lower limit. The only way to verify the assumption that the central light source is the white dwarf alone is to measure the semi-amplitude of the radial velocity curve of the secondary star, K_r , and compare it to that predicted by the photometric model in Table 5. We could also check if this assumption is true using a longer baseline of quiescent observations, as one might expect eclipse timings of an accretion belt to be much more variable than those of a white dwarf. We note, however, that the white dwarf

Table 4. Mean position and extent of the bright spot as defined by equations 1 – 3. ΔZ_2 is calculated according to the definition used by Wood et al. (1986), for ease of comparison.

$\Delta R_d/a$	0.0417
$\Delta\theta$	15°17
$\Delta Z/a$	0.0200
$\Delta Z_2/a$	0.0147
R_d/a	0.2315
θ	43°24

mass given in Table 5 is consistent with the mean white dwarf mass of $0.69 \pm 0.13 M_\odot$ for CVs below the period gap (Smith & Dhillon 1998). Also, Baptista, Catalán & Costa (2000) point out that short-period dwarf novae (specifically OY Car, Z Cha and HT Cas) like OU Vir tend to accrete directly onto the white dwarf, whereas longer-period dwarf novae (IP Peg and EX Dra) usually have boundary layers. We will continue under the assumption that the central eclipsed object is indeed a bare white dwarf.

To determine the remaining system parameters we have used the Nauenberg mass-radius relation for a cold, non-rotating white dwarf (Nauenberg 1972; Cook & Warner 1984),

$$R_w = 7.795 \times 10^6 \left[\left(\frac{1.44M_\odot}{M_w} \right)^{\frac{2}{3}} - \left(\frac{M_w}{1.44M_\odot} \right)^{\frac{2}{3}} \right]^{\frac{1}{2}} \text{ m, (4)}$$

which gives an analytical approximation to the Hamada–Salpeter mass-radius relation (Hamada & Salpeter 1961). If we set $R_w/a = y$, we can rewrite Kepler’s third law in terms of the parameters R_w and y , giving another restriction on the white dwarf radius:

$$R_w = y \left(\frac{GM_w(1+q)P^2}{4\pi^2} \right)^{\frac{1}{3}}. \quad (5)$$

Equations 4 and 5 can be easily solved to give the system parameters, given in Table 5. The secondary radius R_r has been calculated by approximating it to the effective radius of the Roche lobe (Eggleton 1983):

$$R_L = \frac{0.49aq^{\frac{2}{3}}}{0.6q^{\frac{2}{3}} + \ln \left(1 + q^{\frac{1}{3}} \right)}, \quad 0 < q < \infty \quad (6)$$

which is accurate to better than 1 per cent. As the Nauenberg (1972) mass-radius relation assumes a cold white dwarf, we have attempted to correct this relation to a temperature of ~ 14000 K, the approximate temperature given by the blackbody fit below. Wood et al. (1989) and Koester & Schönberner (1986) note that the radius of a white dwarf at 10^4 K is about 5 per cent larger than a cold white dwarf. To correct from 10^4 to 14000 K we have used the white dwarf cooling curves of Wood (1995), which gives a total radial correction of 6.2 per cent. This alternative model is also given in Table 5, and is quoted for all temperature-dependent parameters.

The expected flux from a blackbody $B_\nu(\lambda, T)$ in a passband with transmission function $P(\lambda)$ is (e.g. Wood et al. 1989)

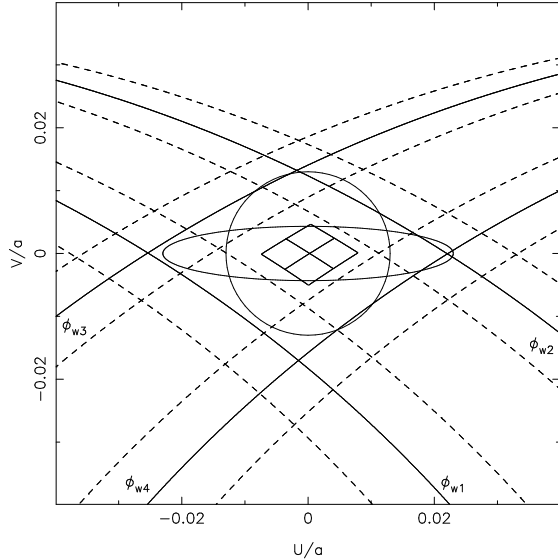


Figure 6. Projection of the white dwarf phase arcs onto the plane perpendicular to the line of sight. U and V are orthogonal coordinates perpendicular to the binary plane. Solid curves correspond to the contact phases of the white dwarf, dotted curves to the rms variations of the phase arcs. The light centre is also plotted surrounded by the solid box corresponding to the rms variations in phase. The projection of the white dwarf and accretion belt centered on $U, V = 0$ are shown for $R_w = 0.013a$ and $R_{belt} = 0.023a$.

$$f = \frac{\int P(\lambda)B_\nu(\lambda, T)d\lambda/\lambda}{\int P(\lambda)d\lambda/\lambda} \cdot \frac{\pi R_w^2}{D^2}, \quad (7)$$

where D is the distance to the star. By fitting a blackbody function to the white dwarf flux in each passband, given in Table 2, we derive a white dwarf temperature of $T_w = 13900 \pm 600$ K and $D = 51 \pm 17$ pc (assuming $R_w = 0.0097 \pm 0.0031 R_\odot$). We would expect some systematic errors to be present in these estimates as we have only used one eclipse and not an averaged lightcurve, so flickering is likely to be a problem.

7 CONCLUSIONS

We have presented an analysis of 5 eclipses of OU Vir, some in superoutburst and some in quiescence. The quiescent eclipses have been used to make the first determination of the system parameters, given in Table 5. Our main conclusions are as follows:

- (i) Eclipses of both the white dwarf and bright spot were observed during quiescence. The identification of the bright spot ingress and egress appears unambiguous.
- (ii) By requiring the gas stream to pass directly through the light centre of the bright spot the mass ratio and orbital inclination were found to be $q = 0.175 \pm 0.025$ and $i = 79.2 \pm 0.7$.
- (iii) Assuming that the central eclipsed object is circular, that its size accurately reflects that of the white dwarf and that it obeys the Nauenberg (1972) approximation to the Hamada & Salpeter (1961) mass-radius relationship, adjusted to $T = 14000$ K, we find that the white dwarf ra-

Table 5. System parameters of OU Vir. The secondary radius given is the volume radius of the secondary's Roche lobe (Eggleton 1983), as defined by equation 6. Parameters left blank in the right-hand column are independent of the model used.

Parameter	Nauenberg (cold)	Nauenberg (14000 K)
Inclination i	79.2 ± 0.7	
Mass ratio $q = M_r/M_w$	0.175 ± 0.025	
White dwarf mass M_w/M_\odot	0.85 ± 0.20	0.89 ± 0.20
Secondary mass M_r/M_\odot	0.15 ± 0.04	0.16 ± 0.04
White dwarf radius R_w/R_\odot	0.0095 ± 0.0030	0.0097 ± 0.0031
Secondary radius R_r/R_\odot	0.177 ± 0.024	0.180 ± 0.024
Separation a/R_\odot	0.73 ± 0.06	0.74 ± 0.05
White dwarf radial velocity $K_w/\text{km s}^{-1}$	75 ± 12	76 ± 12
Secondary radial velocity $K_r/\text{km s}^{-1}$	426 ± 6	432 ± 6
Outer disc radius R_d/a	0.2315 ± 0.0150	
Distance D/pc	51 ± 17	
White dwarf temperature T_w/K	13900 ± 600	

dius is $R_w = 0.0097 \pm 0.0031 R_\odot$ and its mass is $M_w = 0.89 \pm 0.20 M_\odot$.

(iv) With the same assumptions, we find that the volume radius of the secondary star is $R_r = 0.180 \pm 0.024 R_\odot$ and that its mass is $M_r = 0.16 \pm 0.04 M_\odot$. The secondary star is therefore consistent with the empirical mass-radius relation for the main-sequence secondary stars in CVs of Smith & Dhillon (1998).

(v) A blackbody fit to the white dwarf flux gives a temperature $T_w = 13900 \pm 600$ K and a distance $D = 51 \pm 17$ pc with the same assumptions as above. These are purely formal errors from the least-squares fit using estimated errors of ± 0.01 mJy for each flux measurement. Given that we use data from only one eclipse, with a single measurement of the flux from each passband, the actual uncertainties are likely to be significantly larger.

(vi) The accretion disc radius of $R_d/a = 0.2315 \pm 0.0150$ is similar in size to that of HT Cas, for which Horne et al. (1991) derived $R_d/a = 0.23 \pm 0.03$. This is small compared to many other dwarf novae (e.g. Z Cha, which has $R_d/a = 0.334$; Wood et al. 1989), but larger than the circularisation radius (Verbunt 1988, equation 13) of $R_{\text{circ}} = 0.1820a$. We note that this is an unusually small disc radius. It is especially surprising as this disc radius was determined from observations obtained only 20 days after the superoutburst was first reported (Kato 2003).

(vii) The superhump period of OU Vir is $P_{sh} = 0.078 \pm 0.002$ days (Vanmunster et al. 2000), which means OU Vir lies 5σ off the superhump period excess–mass ratio relation of Patterson (1998, equation 8), with the superhump period excess $\epsilon = (P_{sh} - P_{orb})/P_{orb} \sim 0.073$. However, it does not lie on the superhump period excess–orbital period relation either, perhaps indicating that the current estimate of the superhump period P_{sh} is inaccurate.

ACKNOWLEDGMENTS

We thank the anonymous referee for useful comments. We are grateful to Tonny Vanmunster for providing his times of mid-eclipse. WJF would like to thank Timothy Thorroughgood for helpful discussions. WJF, MJS and CSB are supported by PPARC studentships. CAW is employed

on PPARC grant PPA/G/S/2000/00598. ULTRACAM is funded by PPARC grant PPA/G/S/2002/00092.

REFERENCES

Baptista R., Catalán M. S., Costa L., 2000, MNRAS, 316, 529
 Cook M. C., Warner B., 1984, MNRAS, 207, 705
 Dhillon V. S., Marsh T. R., 2001, New Ast. Rev., 45, Issue 1-2, 91
 Dhillon V. S., Marsh T. R., et al. 2003, MNRAS, in preparation
 Eggleton P. P., 1983, ApJ, 268, 368
 Flannery B. P., 1975, MNRAS, 170, 325
 Fukugita M., Ichikawa T., Gunn J. E., Doi M., Shimasaku K., Schneider D. P., 1996, AJ, 111, 1748
 Hamada T., Salpeter E. E., 1961, ApJ, 134, 683
 Horne K., Wood J. H., Steining R. F., 1991, ApJ, 378, 271
 Kato T., 2003, vsnet-alert, No. 7733
 King D. L., 1985, RGO/La Palma Technical Note 31, Atmospheric Extinction at the Roque de los Muchachos Observatory, La Palma
 Koester D., Schönberner D., 1986, A&A, 154, 125
 Lubow S. H., Shu F. H., 1975, ApJ, 198, 383
 Lubow S. H., Shu F. H., 1976, ApJ, 207, L53
 Mason E., Howell S. B., Szkody P., Harrison T. E., Holtzman J. A., Hoard D. W., 2002, A&A, 396, 633
 Nauenberg M., 1972, ApJ, 175, 417
 Patterson J., 1998, PASP, 110, 1132
 Rutten R. G. M., Kuulkers E., Vogt N., van Paradijs J., 1992, A&A, 265, 159
 Smith D. A., Dhillon V. S., 1998, MNRAS, 301, 767
 Smith J. A., Tucker D. L., et al. 2002, AJ, 123, 2121
 Vanmunster T., Velthuis F., McCormick J., 2000, Inf. Bull. var. Stars, 4955
 Verbunt F., 1988, ApJ, 332, 193
 Wood J. H., Horne K., Berriman G., Wade 1989, ApJ, 314, 974
 Wood J. H., Horne K., Berriman G., Wade R., O'Donoghue D., Warner B., 1986, MNRAS, 219, 629
 Wood J. H., Irwin M. J., Pringle J. E., 1985, MNRAS, 214, 475

Wood M. A., 1995, in Koester D., Werner K., eds, European Workshop on White Dwarfs, Lecture Notes in Physics, Volume 443, p. 41